Bioactive Materials 42 (2024) 226–240

Contents lists available at ScienceDirect

Bioactive Materials

journal homepage: www.keaipublishing.com/en/journals/bioactive-materials

Amphiphilic cytokine traps remodel marrow adipose tissue for hematopoietic microenvironment amelioration

Shunshu Deng [a,b,c,d], Shuang Zhang [a,c,d], Tong Shen [a,c,d], Xuanlin Wang [a,c,d], Zehua Gao [a,c,d], Wenchao Zhang [a,c,d], Kai Dai [a,c,e,**], Jing Wang [a,d,e,*], Changsheng Liu [c,d,e,***]

[a] State Key Laboratory of Bioreactor Engineering, East China University of Science and Technology, Shanghai, 200237, PR China
[b] Institute for Regenerative Medicine, Shanghai East Hospital, Tongji University School of Medicine, Shanghai, 200092, PR China
[c] Key Laboratory for Ultrafine Materials of the Ministry of Education, East China University of Science and Technology, Shanghai, 200237, PR China
[d] Engineering Research Center for Biomedical Materials of the Ministry of Education, East China University of Science and Technology, Shanghai, 200237, PR China
[e] Frontiers Science Center for Materiobiology and Dynamic Chemistry, East China University of Science and Technology, Shanghai, 200237, PR China

ARTICLE INFO

Keywords:
Adipocytes
Hematopoiesis
In vivo osteo-organoids
Stem cell factor
Sulfated chitosan
Tissue regeneration

ABSTRACT

Hematopoietic stem cell transplantation (HSCT) is extensively employed in the treatment of hematological malignancies but is markedly constrained by the paucity of hematopoietic stem/progenitor cells (HSPCs). Recent studies have found that marrow adipose tissue (MAT) acts on hematopoiesis through complicated mechanisms. Therefore, the osteo-organoids fabricated *in vivo* using biomaterials loaded with recombinant human bone morphogenetic protein 2 (rhBMP-2) have been used as models of MAT for our research. To obtain sufficient amounts of therapeutic HSPCs and healthy MAT, we have developed amphiphilic chitosan (AC)-gelatin as carriers of rhBMP-2 to the regulate type conversion of adipose tissue and trap hematopoietic growth factors. Unlike medicine interventions or cell therapies, the traps based on AC not only attenuate the occupancy of adipocytes within the hematopoietic microenvironment while preserving stem cell factor concentrations, but also improve marrow metabolism by promoting MAT browning. In conclusion, this approach increases the proportion of HSPCs in osteo-organoids, and optimizes the composition and metabolic status of MAT. These findings furnish an experimental basis for regulating hematopoiesis *in vivo* through materials that promote the development of autologous HSPCs. Additionally, this approach presents a theoretical model of rapid adipogenesis for the study of adipose-related pathologies and potential pharmacological targets.

1. Introduction

Hematopoietic stem cell transplantation (HSCT) is the treatment of choice for numerous malignant hematological diseases [1–3]. However, the limited number of hematopoietic stem cells curtails its widespread use. Hematopoietic stem/progenitor cells (HSPCs) are mainly stored in the bone marrow, and their function and proportion can be regulated by multivariate factors, including cell types, cytokine levels, and matrix stiffness [4]. Marrow adipose tissue (MAT) has garnered significant interest as a critical component of the bone marrow hematopoietic microenvironment in recent research. The mainstream view used to be that the voluminous presence of MAT encroaches upon hematopoietic space, and the bone marrow mesenchymal stem cells (MSCs) would lack important hematopoietic growth factors after adipogenic differentiation [5], thereby impeding hematopoiesis. Conventionally, adipose tissue has been categorized into white adipose tissue (WAT), which serves as an energy reservoir, and brown adipose tissue (BAT), which facilitates energy dissipation. It has been observed that a decline in cells expressing

Peer review under responsibility of KeAi Communications Co., Ltd.
* Corresponding author. State Key Laboratory of Bioreactor Engineering, East China University of Science and Technology, Shanghai, 200237, PR China.
** Corresponding author. Key Laboratory for Ultrafine Materials of the Ministry of Education, East China University of Science and Technology, Shanghai, 200237, PR China.
*** Corresponding author. Frontiers Science Center for Materiobiology and Dynamic Chemistry, East China University of Science and Technology, Shanghai, 200237, PR China.
E-mail addresses: daikai233@foxmail.com (K. Dai), biomatwj@163.com (J. Wang), liucs@ecust.edu.cn (C. Liu).

https://doi.org/10.1016/j.bioactmat.2024.08.032
Received 25 March 2024; Received in revised form 23 August 2024; Accepted 27 August 2024

uncoupling protein 1 (UCP1) within MAT correlates with bone marrow aging [6,7]. Concurrently, Nishio et al. have illustrated that HSPCs co-cultured with human embryonic stem cell-derived BAT, which secrete hematopoietic cytokines such as colony-stimulating factors, erythropoietin, and thrombopoietin, outperforms HSPCs alone [8]. However, WAT is often harmful to hematopoiesis because of the inhibitory effect on osteogenesis [9] and the excessive volume. In addition, aging [10,11], obesity [12–14], leukemia [15,16] can also induce abnormal MAT proliferation. Thus, through regulating the phenotypic conversion and quantity change of MAT, function and number of HSPCs are expected to be intervened directly in the marrow.

Recent reports indicate that MAT is different from BAT or WAT, called yellow adipose tissue [17–19]. Further investigation has revealed that MAT has more interactions with HSPCs and bone tissue, and maintains normal hematopoietic function by secreting adiponectin, leptin and stem cell factor (SCF) under certain circumstances [12,20]. For example, MAT can promote the regeneration hematopoiesis by secreting SCF after irradiation [2]. SCFis known to effectively stimulate cell growth, proliferation, and survival of stem cells by engaging c-kit receptors, and it also supports the preservation of HSPC phenotypes; moreover, it has been implicated in mitochondrial regulation [21], promoting the conversion of white adipocytes into beige adipocytes ($UCP1^+/CD137^+$). We previously constructed recombinant human bone morphogenetic protein 2 (rhBMP-2) triggered *in vivo* osteo-organoids which possessed bone marrow-like structure and served as potential HSPC sources for cell therapy [22]. However, these osteo-organoids, created using gelatin sponges, frequently exhibited excessive fatty infiltration and a reduced proportion of HSPCs. Given the aforementioned impacts of MAT on hematopoiesis, there is a pressing need to develop SCF traps capable of diminishing WAT and augmenting $UCP1^+$ adipose tissue.

Notably, it is available to influence HSPCs of the *in vivo* osteo-organoids through materials [23] or pharmacological intervention in adipose [24–26], while materials strategy for remodeling MAT is not common [27,28]. We need a trap to prevent SCF loss and remodel the adipose tissue through sustained release of effective constituents. Conjugated linoleic acid (CLA) can regulate peroxisome proliferator-activated receptors (PPARs) [29], inhibiting PPARγ and activating PPARα to reduce MSC differentiation into white adipocytes [30–32]. Moreover, our previous research has indicated that sulfated chitosan (SCS) exhibit the heparin-binding domain [33–35], and SCF, a heparin-binding protein [36], can be theoretically trapped. Therefore, we utilized CLA as a small molecule to regulate adipocytes, and combined it with SCS to synthesize amphiphilic nanoparticles. Subsequently, gelatin, the same composition as gelatin sponge, was used as the matrix material, and nanoparticles were used as crosslinkers to synthesize amphiphilic chitosan (AC) composites. After characterizing the material properties of these composites, they were loaded with rhBMP-2 and implanted subcutaneously into mice. After 3–5 weeks, the osteo-organoids were harvested and evaluated by histomorphology, cytology, and molecular biology, and consequently. The composites were identified as multifunctional biomaterials with the ability to regulate adipocyte metabolism and trap growth factors, thereby increasing the proportion of HSPCs. Compared to other intervention methods, this material has a simple composition but creates a suitable microenvironment for HSPCs in a targeted, multi-angle, and effective way. Adipose tissue is not only an important part of the hematopoietic microenvironment, but also participates in metabolic pathways affecting physiological or pathological processes [37–39]. Together, these studies confirmed that the hematopoietic microenvironments of *in vivo* osteo-organoids can be improved by material modification, and also established a controllable adipogenesis model.

2. Results

2.1. Component and structure of materials determine the biological functions

We used ammonium persulfate as an initiator to cross-link self-assembled CLA (Scheme 1A) to form CLA micelles (CLAm). The controlled addition polymerization conditions allowed for about (10.0 ± 2.5)% of free CLA (Figure S 1) to remain in the micelles. Infrared spectra analysis (Figure S 2) confirmed that the C=C double bond was not completely reduced after cross-linking. To enhance the sustained release ability of CLA and trap SCF, we modified SCS on the micelle surface through a dehydration condensation reaction, forming AC nanoparticles (Scheme 1A). Transmission electron microscopy (TEM) images (Fig. 1A) showed that the AC surface was covered by SCS, creating a caged structure that increased the specific surface area for trapping factors while ensuring the release ability of small molecules (Scheme 1B).

We cross-linked gelatin solutions using AC nanoparticles as crosslinkers, followed by lyophilization to form scaffolds (Scheme 1A). Due to micelle agglomeration, CLAm (112.6 nm in Fig. 1B) gelatin scaffolds showed larger crosslinkers, as observed in SEM images (Fig. 1D); on the contrary, AC nanoparticles (211.9 nm in Fig. 1B) acted as single nanoparticles as crosslinkers in AC-gelatin scaffolds because of the better dispersion. This phenomenon was confirmed by the Tyndall effect (Figure S 3A). Specific staining of SCS or lipids (Figure S 3C and D) demonstrated the distribution of AC in the scaffold. Elemental analysis revealed different sulfur content between gelatin scaffolds ((0.206 ± 0.004)%) and AC-gelatin scaffolds ((0.438 ± 0.001)%), confirming the successful modification of SCS. MTT (thiazolyl blue tetrazolium bromide) assay (Fig. 1C) and cell activity staining (Figure S 4) were conducted to test the toxicity of the scaffold leach liquor, which confirmed non-toxicities to MSCs. However, AC-gelatin showed obvious pro-apoptotic effects on adipocytes, and the CLAm-gelatin group did not show any cells due to excessive effects (Figure S 4).

Furthermore, fluorescence imaging (Fig. 1E) revealed that SCF was clearly produced by adipocytes under normal culture conditions. However the AC-gelatin-degrading components, mainly SCS-gelatin aggregates, showed a most concentrated presence of SCF with fewer mature adipocytes, indicating the trapping effect to SCF. This phenomenon was attributed to the controlled release of CLA in the nanoparticles, which induced apoptosis in adjacent adipocytes. Additionally, SCS captured both SCF secreted by live adipocytes and SCF on the surface of dead adipocytes. Overall, AC-gelatin demonstrated adipocyte-killing effects and maintained the concentration of SCF, regardless of adipocyte apoptosis, both of which were sustained and controlled.

2.2. Amphiphilic chitosan composites have material properties compatible with biological functions

Since the mechanical properties of the material affect not only the implantation surgery, but also the MSCs (*e.g.* viscoelasticity [40,41]) or hematopoietic stem cells (HSCs; *e.g.* amphipathy [42,43]), we focused on the properties of composite scaffolds and the wet hydrogels (*i.e.*, scaffolds that absorb water as shown in Figure S 3B) to prepare for use as carriers of rhBMP-2. AC-gelatin demonstrated the highest crosslinking degree while CLAm-gelatin exhibited the lowest (Fig. 2A), influenced by the size of the crosslinkers. Besides, contact angle experiments revealed that AC-gelatin scaffolds displayed superior amphipathy (Fig. 2B). The poor relaxation do harm to MSC adhesion [40,41], but low strength causes a large degree of adipogenic differentiation [44,45], so stress relaxation and rheological experiments were used to evaluate the biomechanical level (Table 1) of wet hydrogels to select the materials with the best properties. Either Gelatin or CLAm-gelatin group showed worse creep resistance, or lower strength (Fig. 2C and D), and besides, the cell adhesion ability (Figure S 5) of AC-gelatin was better than that of

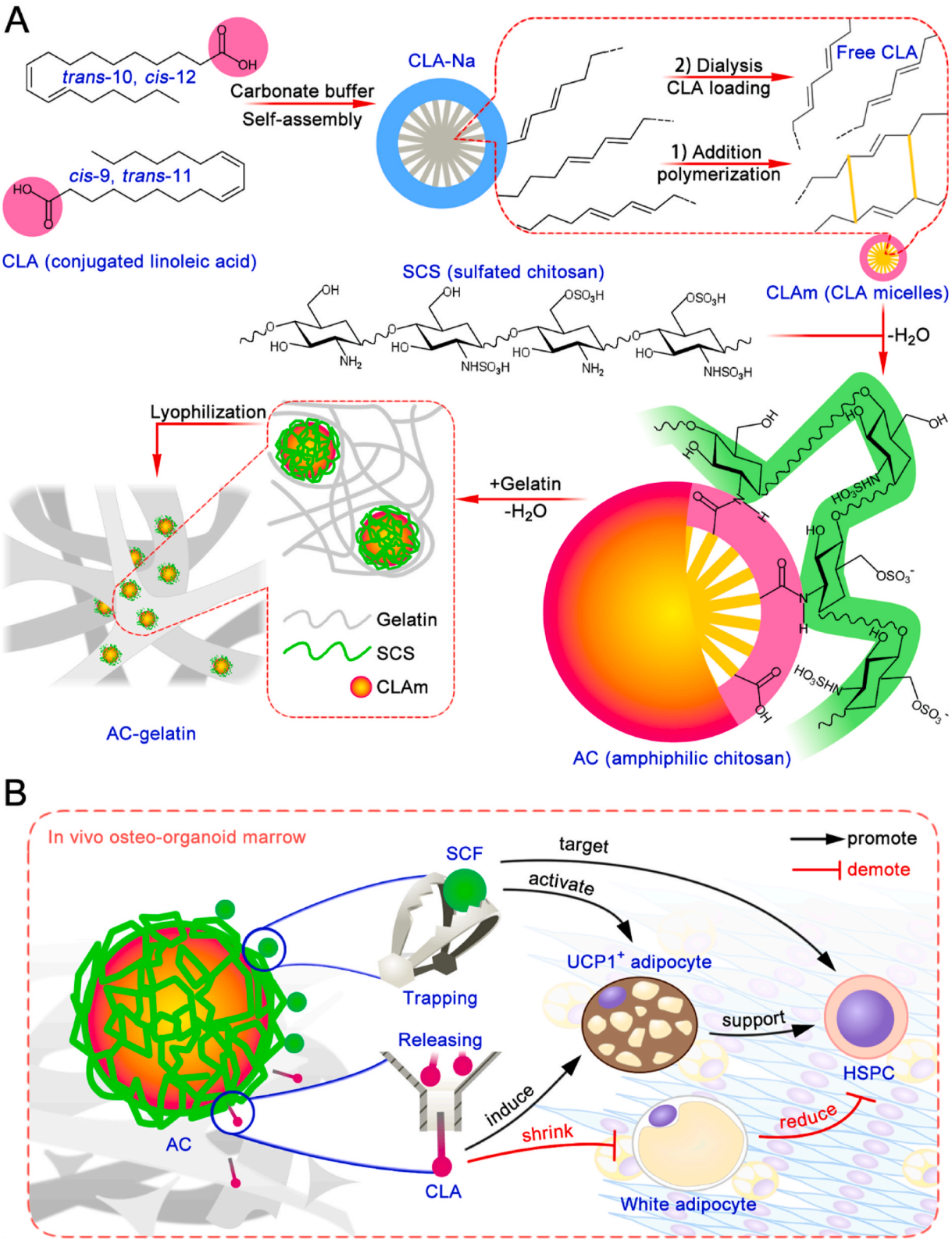

Scheme 1. Schematic of composite synthesis and mechanisms of action *in vivo*. (A) The structural formulae of conjugated linoleic acid (CLA), sulfated chitosan (SCS) and nanoparticle of amphiphilic chitosan (AC), and steps of AC-gelatin scaffold synthesis; the pink circles or rings represent the acidic hydrophilic ends; the azury ring represents the basic hydrophilic end; CLA-Na: sodium CLA. (B) AC-gelatin ameliorates the hematopoiesis of osteoid organs by reducing white adipocytes, increasing brown adipocytes ($UCP1^+$ adipocytes), and trapping stem cell factor (SCF); HSPC: hematopoietic stem/progenitor cells.

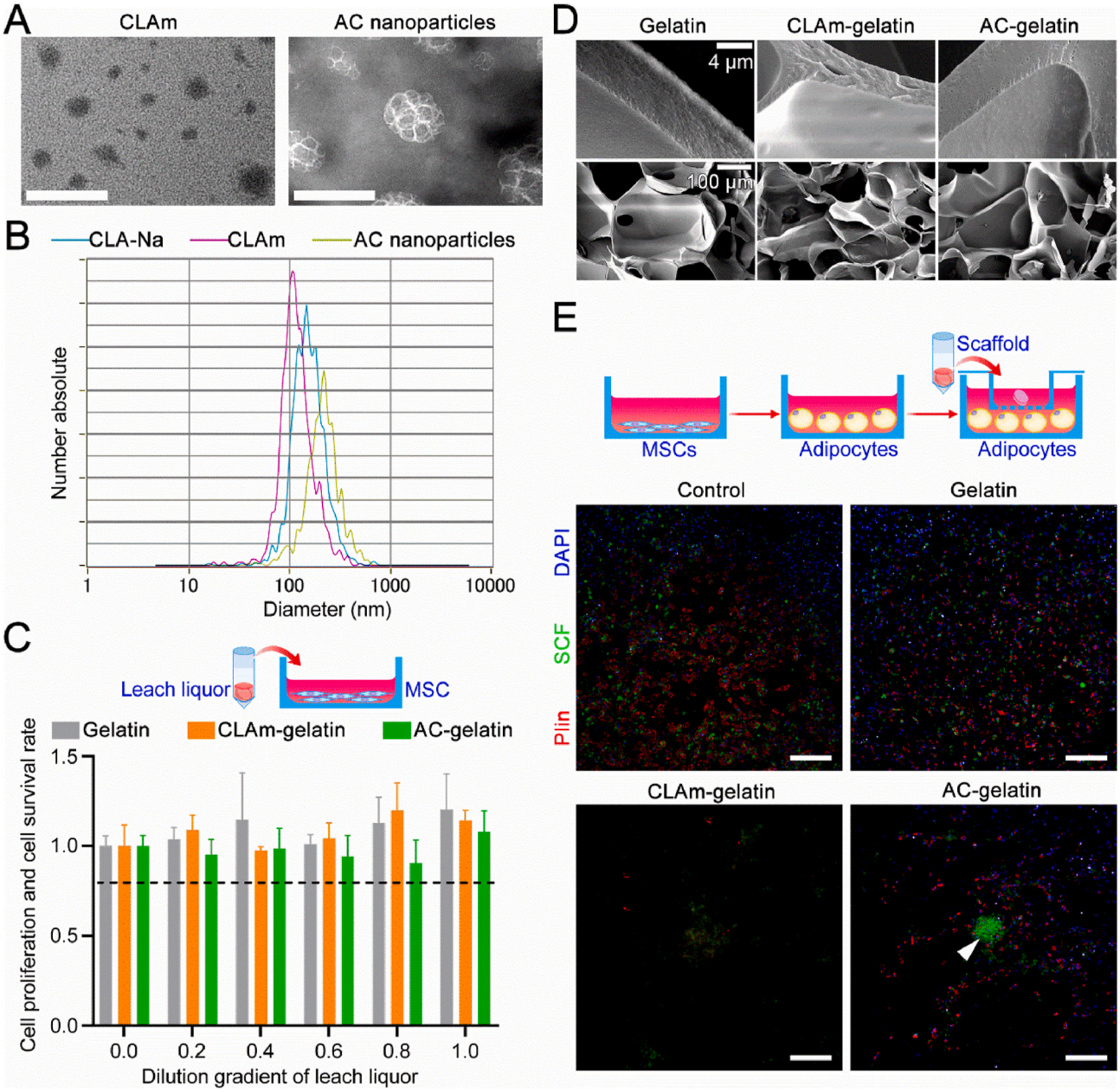

Fig. 1. Multiple biological functions *in vitro* determined by the material component and structure. (A) TEM images; the AC nanoparticles were negatively stained by phosphotungstic acid; both scale bars are 200 nm. (B) Particle size distribution graph. (C) MTT assay for cytotoxicity; 2×10^3 mesenchymal stem cells (MSCs) per wells, 3 days of incubation; the dashed line represents the 80 % rate; error bars: mean ± SD, $n = 3$, number of wells. (D) SEM images. (E) AC aggregates (triangle) successfully trap SCF, while CLAm-gelatin efficiently removes adipocytes in the fluorescence image; MSCs reaching 100 % confluence were induced into adipogenic differentiation for 4 days, and then co-cultured with scaffolds for 4 days; Plin: perilipin, which was used to label lipid droplets, represented adipocytes here; all of the scale bars are 200 μm. AC showed the ability to reduce adipocytes and trap SCF.

traditional gelatin sponge. Therefore, AC-gelatin is more suitable as an rhBMP-2 carrier for the construction of *in vivo* osteo-organoids.

2.3. Amphiphilic chitosan increases the proportion of HSPCs in osteo-organoids

After confirming functions of the composites *in vitro* and their physical properties as implants, we further investigated the hematopoietic potential of these materials loaded with BMP *in vivo* (Fig. 3A). Flow cytometry analysis (Fig. 3B) was performed on the marrow of osteo-organoids constructed using different composites to understand the contribution of different components. Compared with the other materials, the proportion of LSK^+ ($Lineage^-/Sca\text{-}1^+/c\text{-}Kit^+$) cells (Fig. 3C) was maintained at a higher level in AC-gelatin, but the proportion of them decreased in Gelatin group because excess adipose tissue occupied the hematopoietic space at 5 weeks. The results for HSCs were similar to those mentioned above, but the proportion of CLAm-gelatin group increased to close to that of AC-gelatin at 5 weeks (Fig. 3D), because SCF produced from nascent adipocytes after the end of CLA release is more conducive to the proliferation of HSCs. AC-gelatin also had the effect of increasing the $LSK^+/CD150^-/CD48^-$ multipotent blood progenitors (Figure S 6). Furthermore, as for hematopoietic progenitor cells (Fig. 3E), common myeloid progenitor (CMP) and megakaryocyte-erythroid progenitor (MEP) cells also changed to varying degrees due to the effect of the hematopoietic space and SCF, with AC-gelatin group showing a higher proportion in aggregate. Overall, the AC-gelatin-

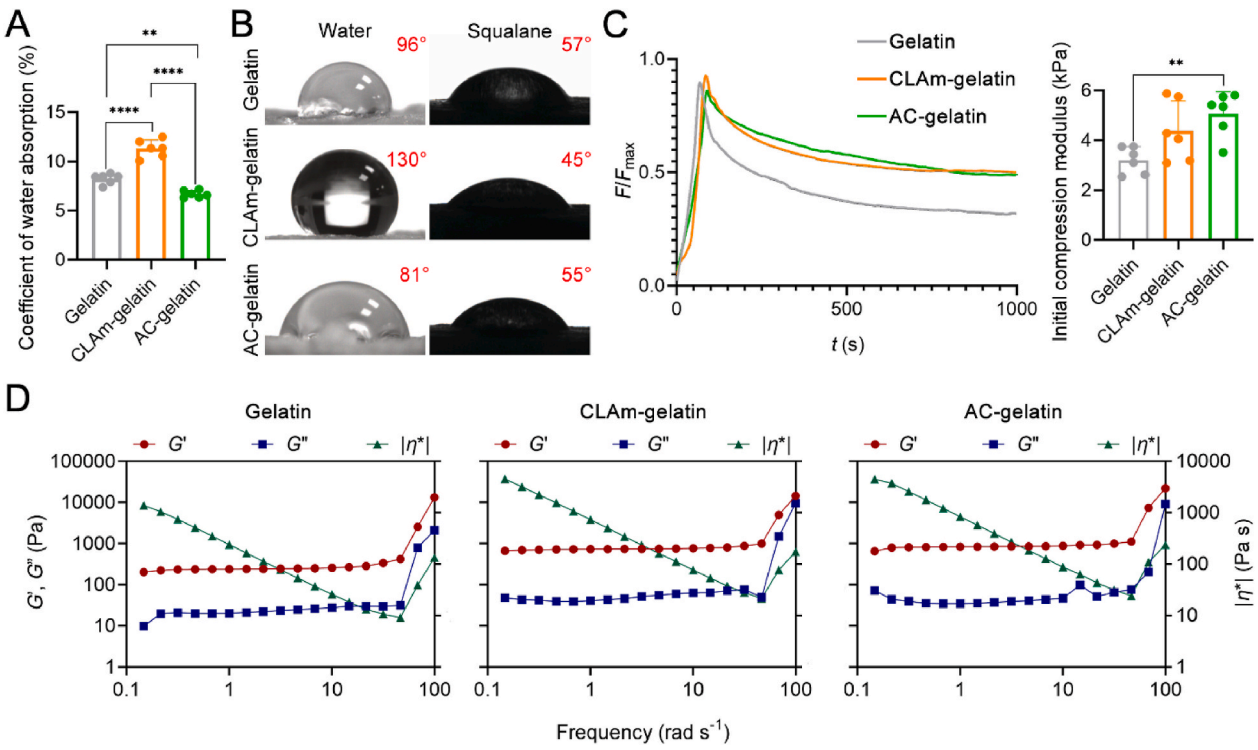

Fig. 2. Material performances associated with biocompatibility and bioactivity. (A) Degree of cross-linking measured by swelling; $n = 6$. (B) The best amphipathy, measured by contact angle (red numbers), of AC-gelatin; squalane was used as the test reagent of oil phase. (C) Stress relaxation and modulus measured ($n = 6$) by compression testing; F: stress; F_{max}: maximum stress. (D) Frequency sweep rheograms of wet hydrogels; G': storage modulus; G'': loss modulus; $|\eta^*|$: shear viscosity. Error bars: mean ± SD; $^{**}p < 0.01$, $^{****}p < 0.0001$, ordinary one-way ANOVA.

Table 1
Material mechanics data of scaffolds.

Physical quantity	Gelatin	CLAm-gelatin	AC-gelatin
v_r/% min^{-1}	4.3	4.0	3.4
$(\tan\delta)_{1\ Hz}$	0.1035	0.07873	0.05047
$\lvert G^*\rvert_{1\ Hz}$/Pa	252.3	758.9	865.0

v_r: relaxation rate; $(\tan\delta)_{1\ Hz}$ and $\lvert G^*\rvert_{1\ Hz}$: loss tangent and shear modulus at the frequency of 1 Hz.

constructed osteo-organoids showed longer term effects of HSC and MEP-dominated progenitor cell proportions maintenance.

2.4. Composites regulate the metabolism of adipocytes in osteo-organoids

Considering the impact of MAT on hematopoietic function, our study proceeded to examine the adipose tissue development during marrow formation through histological analysis. Additionally, MAT was isolated for molecular biology investigations to elucidate the metabolic processes of adipocytes under various influences. Marrow was formed rapidly in AC-gelatin, with noticeable blood vessel formation evident three weeks post-implantation; the CLAm-gelatin composites were in the second place (Fig. 4A). Scaffolds of CLAm-gelatin and AC-gelatin degraded fast (Figure S 7) in simulated body fluid (SBF) due to the immediate release of cross-linked gelatin fibers upon hydrolysis by the crosslinkers, resulting in their good marrow formation. Meanwhile, the decrease of material with marrow development reflected its gradual degradation (Figure S 8). However, after 5 weeks of implantation, the Gelatin group exhibited adipose tissue-filled marrow, while the MAT in the CLAm-gelatin group was minimal (Fig. 4A). The phenomenon of Gelatin group was because the material, without adipose reduction function, was so soft [44,45] that MSCs tended towards adipogenic differentiation. However, thanks to the biological activity of rhBMP-2, the level of osteogenesis in all groups was basically the same (Figure S 9). The statistical plot of the marrow thickness data (Fig. 4B and C), by whose measurement points were uniformly selected, showed a higher degree of pulpefaction and a more uniform thickness in AC-gelatin group.

Finally, the MAT of osteo-organoids at 5 weeks was isolated for adipocyte metabolism-associated genes expression analysis (Fig. 4D): AC-gelatin showed both lipolytic and adipogenic functions, as indicated by significantly higher levels of *Fabp4* (involved in lipolysis) and *Adipoq* (involved in adipogenesis); the higher expression of PPARα compared with PPARγ suggested that adipose progenitors in AC-gelatin tended to differentiate into UCP1$^+$ adipocytes. The expression of UCP1 and CD137 (encoded by *Tnfrsf9*), important markers of brown or beige adipose tissue, indicated a higher level of browning in AC-gelatin group; the highest expression of *Cidea* (involved in maintaining normal adipose metabolism) suggested that AC-gelatin materials had the best potential to prevent insulin resistance. Notably, low levels of *Pi16* (fibrosis-related gene) and *Vapb* (statin metabolism-related gene) were observed in MAT, indicating that MAT produced by these materials was not associated with lesions. In summary, AC-gelatin promoted marrow formation and regulated MAT renewal, metabolism and browning in the long term.

2.5. Amphiphilic chitosan promotes apoptosis of mature adipocytes

To further verify that the sustained release of CLA in AC-gelatin is responsible for the regulation of MAT, we analyzed the contribution of the composite to the mature adipocytes by assessing apoptosis levels. Apoptosis of adipocytes was identified by immunohistochemical images (Figure S 10), which showed aspecific apoptosis in the Gelatin group and adipocyte apoptosis in the other two groups. From the fluorescence apoptotic images (Fig. 5A), we observed that the Gelatin group had abnormally high apoptosis levels at 3 weeks, which was likely caused by the immune response since the poor biocompatibility of the wet hydrogels; more importantly, the sudden release of CLA in the CLAm-

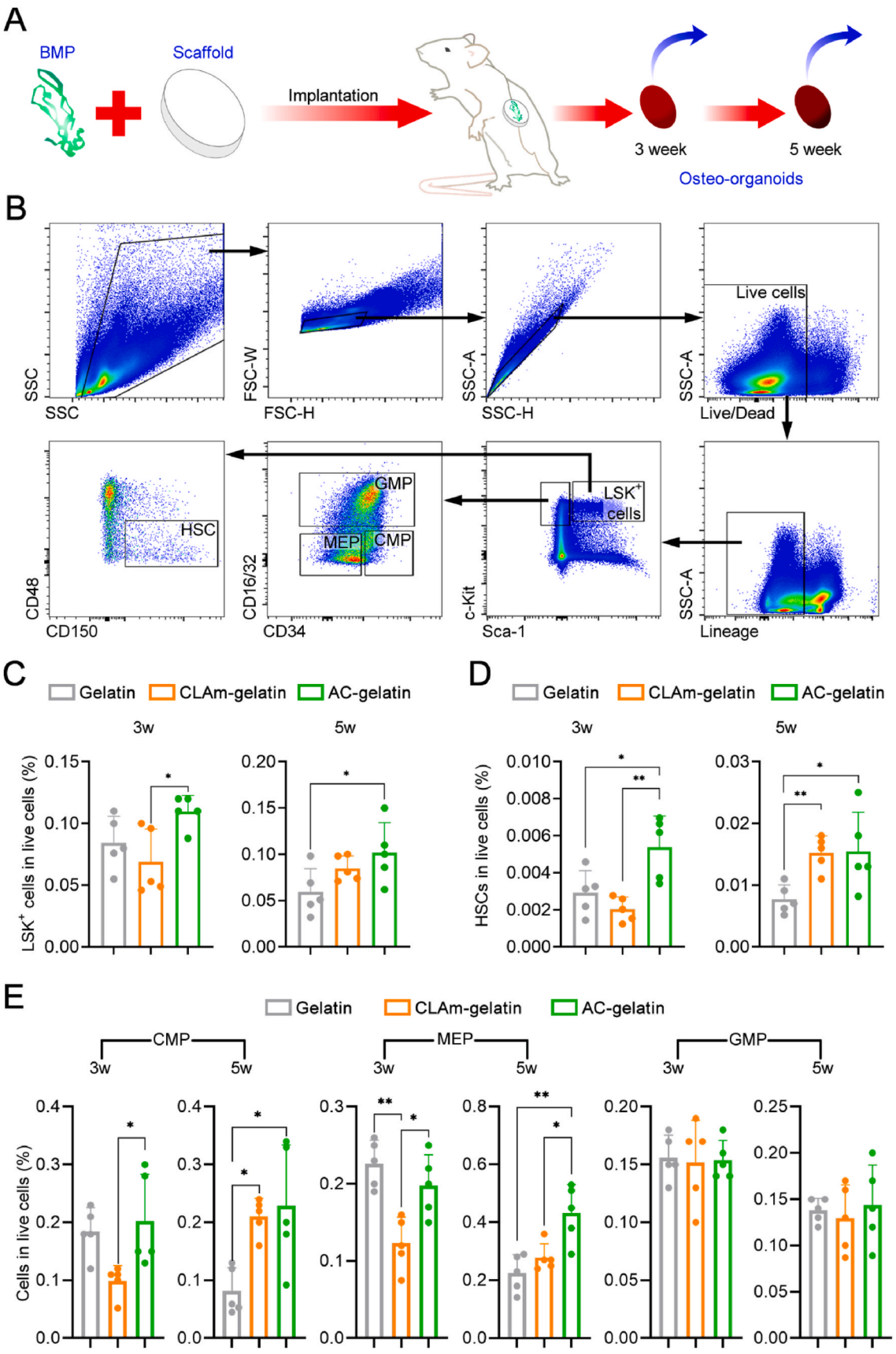

Fig. 3. The addition of AC increased the proportion of HSPCs. (A) Schematic of the constructing and sampling (blue arrows) of osteo-organoids; BMP: bone morphogenetic protein. (B) Gating strategy for flow cytometry analysis of HSPCs. (C–E) Proportion of HSPCs in marrow of osteo-organoids by flow cytometry; LSK^+: $Lineage^-/Sca\text{-}1^+/c\text{-}Kit^+$; HSCs: hematopoietic stem cells; CMP: common myeloid progenitor; MEP: megakaryocyte-erythroid progenitor; GMP: granulocyte-monocyte progenitor. Error bars: mean ± SD; $n = 5$, number of mice; $^*p < 0.05$, $^{**}p < 0.01$, ordinary one-way ANOVA.

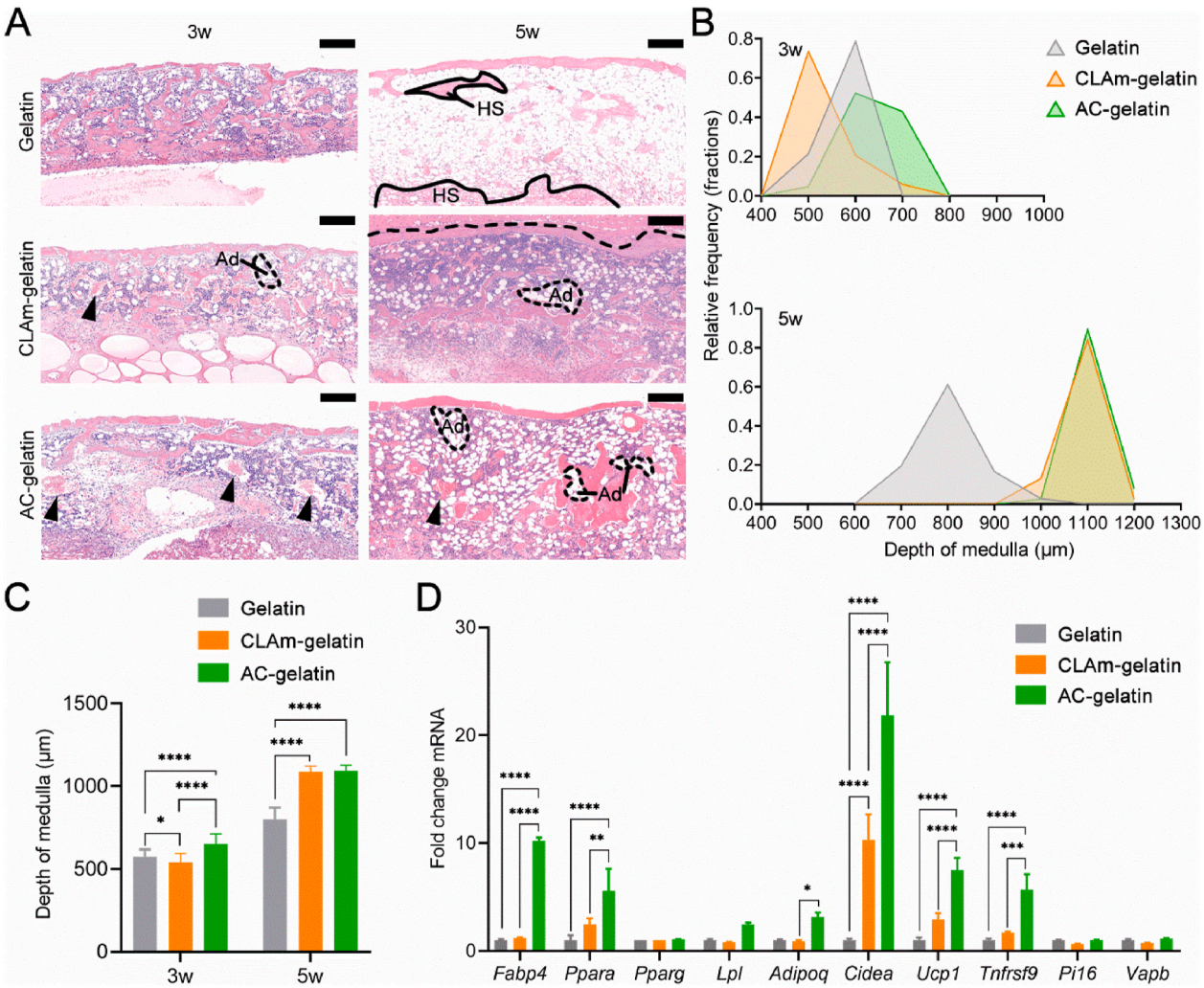

Fig. 4. Metabolic regulation of MAT by AC-gelatin. (A) Hematoxylin-eosin staining showing the better pulpefaction level of AC-gelatin; HS: hematopoietic space; Ad: adipose; the black triangles point to the blood vessels; all scale bars are 200 μm. Distribution (B) and mean statistics (C) of medulla depths in osteo-organoids. (D) Expression levels of adipocyte metabolism-associated genes from MAT at 5 weeks; the isolated MAT was used as samples; AC remodels adipose tissue (*Fabp4*, *Ppara*, *Pparg*), regulates metabolism of MAT (*Lpl*, *Adipoq* and *Cidea*), and significantly promotes browning (*Ppara*, *Pparg*, *Ucp1* and *Tnfrsf9*) without lesions (*Pi16* and *Vapb*). Error bars: mean ± SD; $n = 3$, number of mice; $^{*}p < 0.05$, $^{**}p < 0.01$, $^{***}p < 0.001$, $^{****}p < 0.0001$, two-way ANOVA.

gelatin group caused extensive apoptosis of adipocytes at 3 weeks, including a portion of SCF producing ones; after 5 weeks, the release of CLA ceased and the intervention effect was lost (Fig. 5B). In contrast, adipose tissue in the AC-gelatin group underwent continuous apoptosis, and the space of action was more concentrated than that of CLAm-gelatin group (Fig. 5C). Therefore, it was deduced that AC-gelatin specifically killed adipocytes in contact with AC nanoparticles *in vivo*, and this effect could be stably maintained for long, so sufficient adipocytes with small lipid droplet were preserved to produce SCF, without occupying excessive hematopoietic space.

2.6. Adipocytes shrank without SCF depletion through amphiphilic chitosan

MAT in AC-gelatin was maintained stable in a small volume [24] by the regulation mentioned above. To quantify the changes in adipocyte size and SCF content influenced by different materials, we focused on the mechanism of hematopoiesis improvement by the composites. We investigated lipid droplet sizes and SCF expression *in vivo* through fluorescence co-localization (Fig. 6A). Due to the rapid release of CLA, the number of adipocytes in the CLAm-gelatin group was low at 3 weeks (Figure S 11B). From the distribution data of lipid droplet area (Fig. 6B), the proportion of adipocytes with small lipid droplet in MAT of AC-gelatin group was the highest at 3 weeks, corresponding to the highest proportion of HSPCs at 3 weeks; similarly, the CLAm-gelatin group had the highest proportion of adipocytes with small lipid droplet at 5 weeks, which corresponded to the proportion of HSPCs in the CLAm-gelatin group that increased to the same level as the AC-gelatin group at 5 weeks.

SCF levels in the osteo-organoid marrow of the AC-gelatin group remained consistently high (Fig. 6C) owe to the trapping function of SCS, which was immobilized on the nanoparticles. In the Gelatin group, SCF production from adipocytes increased with adipogenesis, but the proportion of adipose tissue at 5 weeks was too large to make room for hematopoietic cells (Fig. 3C and D); in the CLAm-gelatin group, the production of adipose-derived SCF was low (Fig. 6C) due to controlled adipogenesis until CLA depletion at 5 weeks. Combining these observations, AC-gelatin simultaneously reduced the volume of MAT and captured SCF *in vivo*, so that SCF was no longer solely dependent on adipogenesis (Fig. 6C).

LepR was used to trace the differentiation of MSCs [46] and identify traditional MAT (Fig. 6A),and *e.g.*, $LepR^{+}$ and $Plin^{+}$ cells were considered adipocytes differentiated from MSCs in the marrow. It can be inferred that the uncontrolled adipocyte-killing effects of the

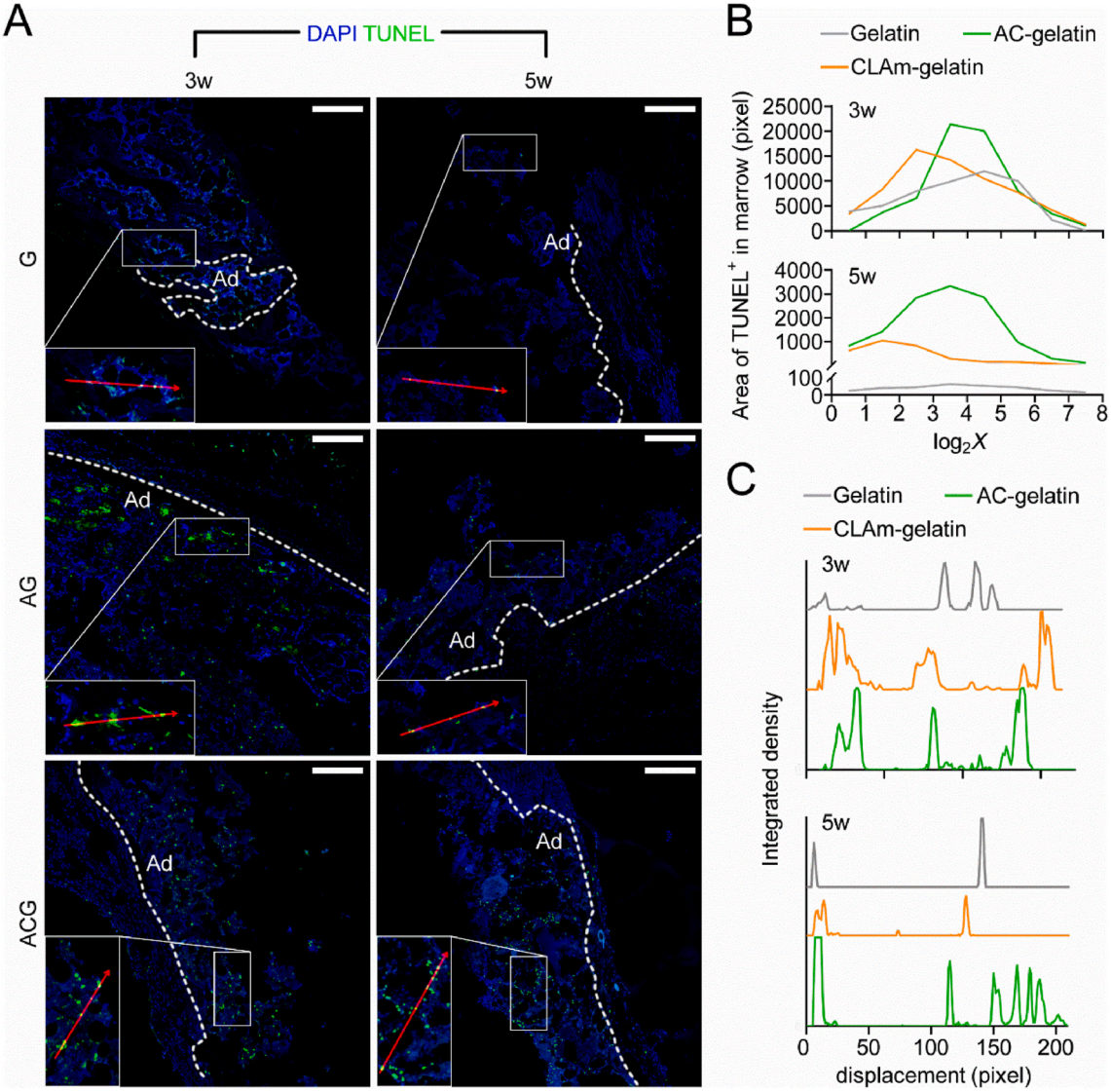

Fig. 5. Material function of continuous apoptosis promotion in mature adipocytes. (A) Apoptotic staining of MAT regions (on the "Ad" side delineated by the dashed line); all scale bars are 200 μm. (B) Distribution of fluorescence intensity of TUNEL$^+$ in Fig. A; *X*: the channel value (0–255) of green. (C) Intensity of TUNEL$^+$ along the direction of the red arrow in Fig. A; the arrow was placed to pass through at least three fluorescence spots, and the lengths of the arrow were kept consistent. The concentrated fluorescence intensity demonstrated the ability of AC-gelatin to release CLA with locality in space and continuity in time.

CLAm-gelatin group led to abnormal adipogenic differentiation (*i.e.*, adipogenic differentiation still occurs when PPARγ is phosphorylated resulting in inactivation, which can hinder the normal function of the adipocytes.) of MSCs at 3 weeks; in contrast, the adipocyte-killing effect of the AC-gelatin group was consistently maintained stable (Fig. 5), which was more conducive to normal metabolism (Fig. 6D). Similarly, the MAT of the Gelatin group at 5 weeks exhibited abnormal metabolism, as indicated by the large proportion of adipose tissue in the marrow cavity (Fig. 4A). Therefore, neither the adipocytes of the CLAm-gelatin-3w group nor the Gelatin-5w group produced more SCF than the AC-gelatin group (Fig. 6D). In short, AC achieves spatial separation of MAT from SCF by capturing SCF while reducing MAT without causing abnormal metabolism.

2.7. Amphiphilic chitosan composites contribute to the browning of MAT and the metabolism of marrow

Based on the aforementioned tests, we confirmed AC-gelatin as an active material with target biological properties. Finally, we investigated the effect of AC-gelatin, compared with traditional gelatin sponge, as materials for constructing osteo-organoids on the subtypes of MAT and the expression levels of other related proteins. MAT in the AC-gelatin group exhibited a significantly higher degree of browning in the osteo-organoids at 5 weeks (Fig. 7A and B). For total protein (Fig. 7C) of whole marrow (without mature erythrocytes), the lower expression of PPARγ (mainly expressed in adipose tissue, and closely related to adipocyte differentiation and insulin resistance.) indicated that AC-gelatin material had a better ability of anti-adipogenesis compared to gelatin sponge; the lower expression of CDK5 (a key regulator of cell cycle progression that leads to phosphorylation of PPARγ) suggested a lower level of ectopic lipid deposition [26] in the AC-gelatin group, which supported the function of ACin reducing insulin resistance; the high expression of PCG-1α (a key factor in the thermogenesis of adipocytes, participating in adipogenesis and regulating maturation.) at 5 weeks also corresponded to the browning of MATin the AC-gelatin group.

Additionally, the differences in the expression of adipose-related proteins (Fig. 7D) in the osteo-organoids compared with in the native bone (tibiae were selected for its higher content of MAT [47].) were further investigated. The results (Fig. 7E) showed that the expression of

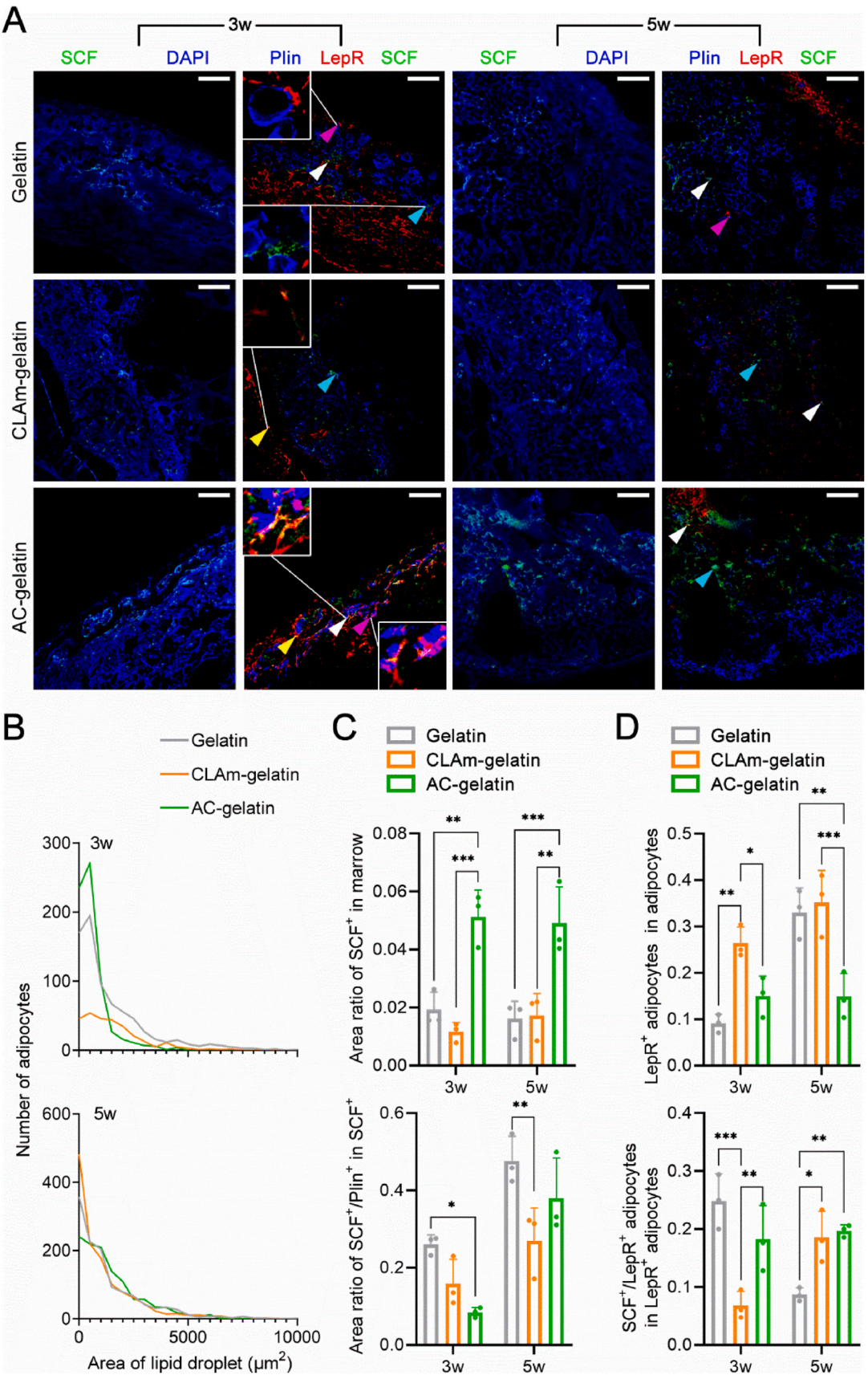

(caption on next page)

Fig. 6. SCF maintenance and inhibition of abnormal adipogenic differentiation from MSCs by AC composites. (A) Fluorescence colocalization imaging of osteo-organoid marrow derived from the transgenic (*Lepr* ^{Cre}; *R26* ^{tdTomato}; *Scf* ^{GFP}) mice with C57BL/6 backgrounds; LepR: leptin receptor, the marker of native bone marrow-derived MSCs as well as adipocytes from MAT; the pair of images in each group belongs to the same section; all scale bars are 200 μm. (B) Frequency distribution of lipid droplet size of osteo-organoid marrow in Fig. A; the area of the similar oval enclosed by Plin was counted; the smaller the adipocytes, the more marrow cavity left for HSPC proliferation. (C and D) Quantitative analysis on SCF and LepR in Fig. A. The triangles point to the colocalization the corresponding color; *e.g.*, the white triangle represents the colocalization of the Plin, LepR and SCF; AC successfully reduced adipose and trapped SCF *in vivo*; the abnormal differentiation of MSCs into adipocytes seldom produced SCF, while AC prevented this abnormality. Error bars: mean ± SD; $n = 3$, number of mice; $^{*}p < 0.05$, $^{**}p < 0.01$, $^{***}p < 0.001$, two-way ANOVA.

most proteins in AC-gelatin group was basically equal to that in tibia group. The proteins related to insulin resistance (promoted by DPPIV or resistin while inhibited by adiponectin) were basically uniformly low-expressed or high-expressed in the AC-gelatin group and the Tibia group. The expression of pentraxin 2, a protein with anti-fibrotic potential [48], was even higher in the AC-gelatin group than in the tibia bone marrow; the significantly higher expression of IGFBP-3 in AC-gelatin compared to the native bone suggests a role of MAT in promoting tissue regeneration (Figure S 12); the immune-related proteins, such as C-reactive protein and ICAM-1, were basically low expressed in all groups. Therefore, it can be inferred that ACG had a stable tissue regeneration function preventing tissue fibrosis caused by immune dysregulation. In conclusion, AC-gelatin demonstrated the ability to reduce adipose and promote browning of MAT, thereby improving the metabolic level and tissue repair ability of the marrow in osteo-organoids.

In summary, under the action of AC-gelatin, the adipose tissue was modified, i.e., the shrink of lipid droplets (Figs. 4A and 6B), the browning of adipocytes (Figs. 4D and 7A, B and C) and the cure of insulin resistance (Figs. 4D, 6D and 7D and E). These are mainly attributed to the sustained release of CLA in AC nanoparticles (Fig. 5 and Figure S 7), which upregulated PPARα and PCG-1α and increased UCP1^{+} adipocytes generating enhanced metabolism and promoted lipolysis. Additionally, the amphiphilic cytokine traps had the function of capturing SCF (Figs. 1E and 6C) and the potential for soft tissue repair (Figs. 4 and 7D and E and Figure S 12), which enhanced the hematopoietic regeneration of osteo-organoids (Fig. 3 and Figure S 6).

3. Discussion and conclusion

The results presented above demonstrate that the traps based on AC are bioactive hydrogels capable of controllably reducing WAT, promoting browning of adipocytes, and trapping SCF over an extended period. Thereby these hydrogels increased the hematopoietic space, improved marrow metabolism, prolonged the role of cytokines, and finally ameliorated hematopoiesis. The action process of BMP-2 loaded AC-gelatin implants *in vivo* is as shown in Scheme 1B: that is, with the invasion from tissue fluid and cells, the matrix gradually disintegrates and AC contact with mature adipocytes; subsequently, the effects on HSPCs are prolonged by trapping SCF; at the same time, the regulation of WAT promotes browning and reduces the direct or indirect (by inhibiting osteogenesis) drain on hematopoietic space; finally, through the combined action of SCF, hematopoietic space and UCP1^{+} adipose tissue, the proportion of HSPCs increases. Moreover, not only the presence of adipocytes, but PPARγ on the surface of HSPCs has been also found to affected hematopoiesis [49], and therefore, CLA, a regulator of PPARs, also contributes directly to hematopoietic enhancement. However, the bone marrow hematopoietic microenvironment is multifactorial and complex in its interactions [11,50–52]; thus, our studies have primarily focused on the SCF and spatial considerations, in conjunction with the active design properties of materials, to develop optimal biomaterials for constructing osteo-organoids. These materials are simple to synthesize and straightforward to manipulate, addressing the issue of excessive fatty infiltration and limited hematopoietic function associated with abnormal metabolic levels [22] in traditional *in vivo* osteo-organoids. Furthermore, these studies offer the potential to enhance the functionality of osteo-organoids through material modification.

It is worth mentioning that in addition to SCF, there are other factors binding the heparin domain that are beneficial to the hematopoietic microenvironment in different ways, such as fibroblast growth factors (a heparin-binding protein with the potential to enhance hematopoietic differentiation and induce browning of adipocytes [53–55]), vascular endothelial growth factor [33,35,56] and granulocyte/macrophage colony-stimulating factor [5,57,58]. Therefore, the trap itself has the ability to capture various growth factors, which will be expected to make contributions to tissue repair. Both bone marrow and adipose tissue, as soft tissues rich in stem cells, play critical roles in regenerative medicine. The significance of bone marrow in HSCT, immune recovery, and stem cell therapy is well-established; meanwhile, the utility of adipose tissue in filling organ defects and plastic surgery [28,59] has been gaining increased attention. Hence, osteo-organoids with a high proportion of HSPCs, metabolically active adipose tissue, and an abundance of high-quality stem cells [22,60] are urgently needed. The application of AC-gelatin expands the regulation of MAT and hematopoiesis based on original studies [2,12,50,61,62]. The amphipathic material properties conducive to the differentiation and self-renewal of HSPCs [42] satisfy the favorable conditions required for the *in vitro* culture of human HSPCs [43]. Moreover, the etiology of fatty infiltration is multifaceted [63] with inflammation-induced adipocyte migration [39] and ectopic lipid deposition [64] being particularly undesirable. Owing to the sulfonic groups, AC nanoparticles possess anti-fibrotic potential [48] during tissue repair. Therefore, AC-gelatin, as a cytokine trap with moderate viscoelasticity, ensures stem cell adhesion without promoting excessive adipogenic differentiation. Furthermore, the ability of CLA to solubilize vitamin A [65] and the drug loading capacity of CLAm [66], the role of SCS in enhancing vascularization [35] and scavenging reactive oxygen species [67], as well as the improved metabolic level by MAT browning, all contribute to maintaining a youthful marrow state. The development of AC-gelatin thus represents a significant step toward reversing senescence.

From a foundational research perspective, not only the disease such as insulin resistance [13,68,69], cardiovascular disease [13,70], endocrine disorders [13,71], and liver cirrhosis [68,72], but also the aging of the bone marrow [38,64], is closely related to the metabolism of lipids. Compared with traditional gelatin sponges, AC-gelatin scaffolds exhibit superior strength and degradability, enabling the generation of larger osteo-organoids without obvious fusion between material and tissue, which facilitates the acquisition of ample adipose tissue for molecular biology studies. Using AC-gelatin, a substantial amount of adipose tissue with a healthy metabolic state can be obtained within one month. Additionally, adipose tissue remodeled by AC-gelatin exhibits high levels of browning, low insulin resistance, and reduced fibrosis processes. And UCP1^{+} adipose tissue, a unique subtype of adipose tissue that expends energy in the form of heat production from lipids, is the key to improve the metabolism and reduce WAT [27,73–75]. Thus adipocytes in this microenvironment are capable of promoting regeneration, enhancing metabolism, and resisting fibrosis. Collectively, these composites demonstrate activity in tissue repair, indicating that the novel matrix for osteo-organoids has potential applications in regenerative medicine.

In conclusion, we have purposefully designed cytokine traps based on AC to consider the multifaceted effects of MAT on hematopoiesis and to construct osteo-organoids that regulate adipocytes to increase the

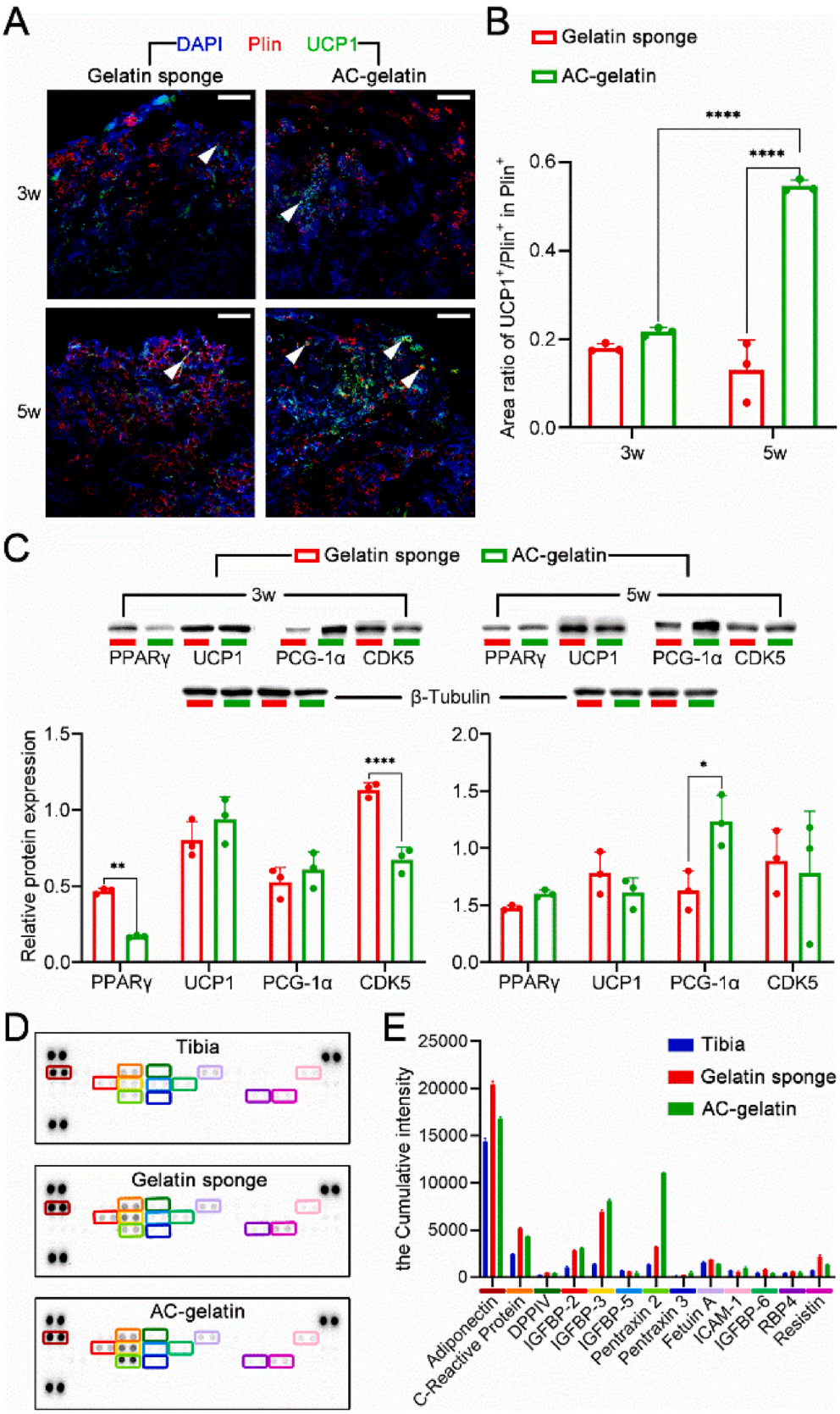

Fig. 7. Changes, especially browning, in the expression of proteins about adipocyte metabolism in marrow induced by AC-gelatin composites. (A) Fluorescence colocalization imaging of the UCP1^{+} adipocytes through represented by UCP1 and Plin (white triangles); all scale bars are 200 μm. (B) MAT browning promotion by AC-gelatin at 5 weeks in statistics of Fig. A. (C) Protein expression tests of osteo-organoid and bone marrow by Western blotting; β-tubulin, a protein expressed stably in adipocytes, was used as the internal reference. (D) Protein expression tests of whole marrow by protein microarray (Proteome Profiler Mouse Adipokine Array Kit, R&D Systems) and the quantified data (E). Error bars: mean ± SD; $n = 2$ (Fig. E, number of wells) or 3 (the others, number of mice); *$p < 0.05$, **$p < 0.01$, ****$p < 0.0001$, two-way ANOVA.

proportion of HSPCs. AC-gelatin, with its dual role as a material structure and molecular function, represents a biological material with a simple hierarchy and is produced through a convenient synthesis process. This study presents a set of available methods for enhancing the hematopoietic capacity of osteo-organoids by intervening in the development of MAT, which may be applied to regenerative medicine related to soft tissue repair or as a designable and efficient adipose production model for the study of adipocyte-related pathophysiological processes and the exploration of drug targets.

4. Experimental section

4.1. Material preparation and osteo-organoid construction

The AC-gelatin composite was cross-linked using CLAm, SCS (synthesized in bulk in laboratory [35]), and gelatin via EDC/NHS coupling chemistry. In brief, CLA was added to carbonate buffer (pH 10.5) and stirred until it self-assembled; then, ammonium persulfate was added into the stirring emulsion (2.5 % (*V/V*)) as an initiator to a concentration of 1 mg/mL, and the reaction was carried out overnight at room temperature; after removal of impurities by dialysis, the emulsion was frozen and lyophilized to obtain the micelle powder as CLAm. Subsequently, 2.45 mg/mL SCS solution, containing 2.5 mg/mL NHS, was mixed with 7 mg/mL CLAm emulsion, containing 25 mg/mL EDC, in a 2:1 vol ratio, and the reaction was carried in shaker (80 rpm) for 30 min at 37 °C; finally, the above mixture was mixed with 100 mg/mL gelatin solution in a 3:2 vol ratio, and the composite hydrogel was obtained after cross-linking at 4 °C for 48 h. Through removing the composition of SCS or CLAm in the reactant system, CLAm-gelatin or gelatin hydrogels were obtained accordingly.

To obtain scaffolds for constructing osteo-organoids, the composite hydrogels were frozen and lyophilized, followed by repeated washing in sterile water to remove catalysts. Having absorbed water, the scaffolds were frozen at −20 °C until used. The scaffolds were lyophilized and cut into sizes of 10 mm × 5 mm × 5 mm, and then 30 μL rhBMP-2 (1 mg/mL; Shanghai Rebone Biomaterials Co.) was added. Then the BMP-loaded scaffolds were frozen and lyophilized and implanted into the back of mice. After a certain period of time, the osteo-organoids were obtained from mice. Similarly, osteo-organoids derived from gelatin sponge scaffolds were also constructed by the same methods.

4.2. Animal model

For these studies, the C57BL/6 (wild type) mouse strain (8 weeks, males) was selected. All mice were purchased from and housed in Shanghai Shengchang Biotechnology Co., Ltd. at 22–23 °C on a 12 h light/dark cycle with free access to water and food, as indicated. A multifluorescent reporter mouse line was constructed by crossing *Lepr* ^{Cre}; *R26* ^{tdTomato} mice with *Scf* ^{GFP} mice [2]. All experimental procedures were approved by the Animal Care and Use Committee of the East China University of Science and Technology (approval No. ECUST-2022-053). All efforts were made to minimize animal suffering.

4.3. Characterization of materials

4.3.1. Mechanical characterization

All mechanical tests were performed using wet hydrogels, which were prepared as cylindrical specimens (Ø20 mm × 5 mm). Unconfined compression tests were then performed on specimens at deformation rates of 1 mm min^{-1}, until 30 % compressive strain; then maintained for 10^3 s and the corresponding stress was measured over time (stress-relaxation test). Meanwhile, the initial elastic modulus was quantify during the first 10 s. Next, we defined the relaxation rate (v_r) as the ratio of the maximum amount of stress drop to the time consumed to quantify the stress-relaxation behavior. Hydrogels were discarded after each test. Frequency sweep of rheology was performed from 0.1 to 100 rad s^{-1} at 1 % strain and 37 °C, and storage and loss moduli were measured to obtain the composite viscosity curve. In addition, the loss tangent (tan δ) and shear modulus ($|G^*|$) at 1 Hz were selected as the viscoelastic indices of the hydrogel by observing the dynamic measurements.

4.3.2. Spectroscopy characterization

To confirm the successful crosslinking, infrared spectroscopy was used to detect CLA micelles before and after crosslinking. CLA-Na was used for the sample before cross-linking in order to maintain the micelle morphology.

Ultraviolet (UV) spectrophotometry was used to further confirm the uncrosslinked CLA content, and 90 % (*V/V*) ethanol was used as the solvent. Based on the UV spectrogram, detection wavelength was set at 229 nm (Figure S 1A), and different concentrations of CLA were dissolved in solvent to obtain the standard curve ($r \approx 0.9991$; Figure S 1B). Different masses of CLAm were then ultrasonically dispersed in the solvent and centrifuged through 1 kDa ultrafiltration tubes at 3000×*g* for 30 min, that is, the solution was tested for absorbance.

4.3.3. Microscopy characterization

CLAm and AC, purified by dialysis method, were added onto the copper mesh to prepare the sample, and recorded by TEM (JEM-2100; JEOL, JPN). After the scaffolds snapped off using liquid nitrogen, their cross-sections were photographed by SEM (G4 UC; Helios, GER).

Slice samples of scaffolds were photographed using an all-in-one fluorescence microscope after sequential staining with oil red O and toluidine blue. For the tissue section samples, confocal microscopy was used.

4.3.4. Other properties of materials

For particle size testing, CLA-Na was dispersed in water vs. CLAm and AC in carbonate buffer to prepare samples (pH = 10.5). For the contact angle test, the scaffolds were prepared as Ø20 mm circular samples; squalene, a biocompatible organic molecule without hydrophilic groups, was used as the test reagent for the oil phase. For the water absorption experiment, the scaffold was weighed in mass (m) after water absorption for 48 h at room temperature, and then lyophilized for 48 h and reweighed in mass (m_0), and the water absorption coefficient (Q) was calculated using the following equation.

$$Q = \frac{m - m_0}{m_0} \tag{1}$$

4.4. Biological characterization in vitro

4.4.1. Degradation experiments

A sterile Ø15 mm × 5 mm cylindrical sample (Gelatin, CLAm-gelatin, or AC-gelatin scaffold) was divided into two parts and placed into a 15 mL centrifuge tube. Next, 10 mL of simulated body fluid was added to each tube. The tubes were then placed on a constant temperature shaker at 37 °C and 80 rpm until sample degradation. For obtaining the leach liquor, in brief, each of the above sample, divided into four parts, was shaken under the same conditions for 48 h, but the buffer was changed to 5 mL of minimal essential medium α (Gibco). After centrifugation at 3000×*g* for 5 min to remove sediment, the supernatant was supplemented by other components to prepare the culture medium.

4.4.2. Cell experiments

The cells were MSCs derived from osteo-organoids constructed by rhBMP-2 loaded gelatin [76,77]. For cell attachment experiments, either gelatin sponge or AC-gelatin was placed in 4 °C culture medium (CM-M131; Wuhan Procell Life Science&Technology Co.) until the materials sank; the wet hydrogels were placed in well plates, and the cell suspension was dropped onto the top surface of the hydrogels. After 8 h, the medium was changed, and the hydrogels were incubated for 72 h, followed by fixation with 1 % paraformaldehyde for 1 h. Finally, cells on

the hydrogel were stained sequentially with phalloidin-FITC and DAPI, and were ready for imaging analysis.

For transwell co-culture experiments, an equal amount of scaffolds was placed in a chamber and placed on 100 % confluent adherent MSCs. Both the cells and the materials were immersed in adipogenic differentiation induction medium. After 2 weeks of incubation following the instructions of the kit (Mesenchymal Stem Cell Adipogenic Differentiation Medium; Cyagen Biosciences Inc.), the medium was removed, and the immunofluorescence staining of perilipin and TUNEL staining were performed according to requirements. The images with the most obvious phenomenon in six repeated trials were used for the presentation of the results.

4.5. Histological characterization

Once after removal from the body, the osteo-organoids were fixed in 4 % paraformaldehyde for 4 h, and then incubated in EDAT decalcification solution (Servicebio) until bone softening. Finally, the tissues were dehydrated, embedded and used for the preparation of slice samples. For hematoxylin-eosin staining, the samples were 4-μm paraffin sections, and the imaging instrument was an inverted microscope (DMi8; Leica, GER). The samples were 60-μm frozen sections for immunofluorescence or 6-μm frozen sections for TUNEL assay, and the imaging instrument was a confocal microscope (A1R; Nikon, JPN).

Sections from the coronal sagittal plane were selected. The area with the average density and quantity of adipose was used to normalize the entire osteo-organoids. For apoptosis images, since the specific location of each adipocyte cannot be well determined, the area with the highest adipose density and quantity was used to represent the entire osteo-organoid. Each lipid droplet was marked by circles based on fluorescence signals, followed by cell counting (mature adipocytes and $LepR^{+}$ cells) and area calculations (SCF and marrow) using ImageJ software.

Marrow thickness was measured as follows: from the cortical bone to the interface between tissue and material, the measured area was subjected to “Local Thickness” (ImageJ) and 40 points were uniformly taken.

4.6. Molecular biologic characterization

4.6.1. Quantitative real-time PCR

To extract total RNA from the MAT of osteo-organoids, the following procedure was followed. Osteo-organoids were fully ground using a digestive enzyme mixture [62,77] at 37 °C and the supernatant was centrifuged at 300×*g* for 5 min. After washing and centrifugation at 4 °C, 800×*g* for 10 min, the separated pellets and fats were dispersed using 1 mL Trizol (Takara), and the mixture was lysed on ice for 5 min. Finally, the procedure of the kit was continued. A real-time PCR instrument (CFX96; USA) was used for qPCR testing.

4.6.2. Quantitative and semi-quantitative analysis of protein

To extract total protein from the marrow of osteo-organoids, the following procedure was followed. Osteo-organoids were rapidly ground with red cell lysis buffer (Beyotime) at 4 °C and the supernatant was removed after centrifugation at 800×*g* for 5 min. Then the separated pellets and fats were dispersed using RIPA (radio immunoprecipitation assay; Beyotime) lysis buffer (with 1 % (*V/V*) phenylmethyl-sulfonyl fluoride), and the mixture was lysed on ice for 5 min. Finally, the suspension was centrifuged (5424 R; eppendorf, GER) at 15000 rpm for 20 min to obtain protein solution.

The following steps were continued: protein denaturation, electrophoresis, membrane transfer, antibody incubation, and imaging. The above protein solution was used as the sample for western blotting and protein microarray.

The osteo-organoid was fully ground in a phosphate buffered saline solution at 4 °C, then centrifuged at 3000×*g* for 5 min. The supernatant obtained was used as the sample for enzyme-linked immunosorbent assay (ELISA), and then the experimental operation followed the instructions in the Quantikine ELISA Kit (R&D Systems).

4.7. Flow cytometry

For sample preparation, osteo-organoids were fully ground with cell staining buffer (BD) and the supernatant was removed after centrifugation at 300×*g* for 5 min. Then the separated pellets were dispersed using red cell lysis buffer for 5 min and centrifuged again. After washing the cells with staining buffer, they were stained using fluorescent antibodies and analyzed by flow cytometry.

The cell aliquots were incubated using phycoerythrin (PE) conjugated CD150, PE-Cy7 (Cyanine 7) conjugated c-Kit, Alexa Fluor 700 (AF700) conjugated stem cell antigen-1 (Sca-1), Brilliant Violet 510 (BV510) conjugated CD48 (BioLegend); BV605 conjugated CD16/32, BV421 conjugated CD34, peridinin-chlorophyll-protein (PerCp)-Cy5.5 conjugated Lineage (BD), and allophycocyanin (APC)-Cy7 conjugated Live/Dead (eBioscience) for 30 min at 4 °C temperature in the dark. After washing the cells with staining buffer, they were resuspended and prepared for testing. The flow cytometry analysis was operated on CytoFLEX LX flow cytometer (Beckman Coulter). The data were analyzed using FlowJo X (Three Star).

4.8. Statistical analysis

Statistical analyses were performed using GraphPad Prism software (version 8.0; GraphPad, La Jolla, CA, USA). The statistical significance of differences between groups was calculated by one-way ANOVA followed by Tukey’s multiple comparison test, or two-way ANOVA followed by Bonferroni’s multiple comparison test as indicated. *p* and *n*-values for the statistical tests are provided in the respective figure legends; the *p*-value less than 0.05 was considered statistically significant.

Ethics approval and consent to participate

All procedures were approved by the Animal Care and Use Committee of the East China University of Science and Technology. The ethical approval number was ECUST-2022-053.

CRediT authorship contribution statement

Shunshu Deng: Writing – original draft, Visualization, Software, Investigation, Formal analysis, Data curation, Conceptualization. **Shuang Zhang:** Validation, Resources, Methodology, Conceptualization. **Tong Shen:** Software, Investigation, Formal analysis. **Xuanlin Wang:** Investigation, Data curation. **Zehua Gao:** Methodology, Investigation. **Wenchao Zhang:** Investigation. **Kai Dai:** Writing – review & editing, Software, Resources, Methodology, Funding acquisition, Conceptualization. **Jing Wang:** Writing – review & editing, Resources, Project administration, Funding acquisition. **Changsheng Liu:** Resources, Project administration, Funding acquisition.

Declaration of competing interest

The authors declare that they have no known competing financial interests or personal relationships that could have appeared to influence the work reported in this paper.

Acknowledgements

We thank the research group of Prof. R. Yue at Tongji University for his kindly gifts of transgenic mice with fluorescence-labeled reporter genes. This work was supported by the Basic Science Center Program of National Natural Science Foundation of China (No. T2288102), the Key Program of the National Natural Science Foundation of China (No. 32230059), the National Natural Science Foundation of China (No.

32301123), the Foundation of Frontiers Science Center for Materiobiology and Dynamic Chemistry (No. JKVD1211002), the Wego Project of Chinese Academy of Sciences [No. (2020) 005], the China Postdoctoral Science Foundation (No. 2022M721147), the Project of National Facility for Translational Medicine (Shanghai) (No. TMSK-2021-134), and the Peak Disciplines (Type IV) of Institutions of Higher Learning in Shanghai.

Appendix A. Supplementary data

Supplementary data to this article can be found online at https://doi.org/10.1016/j.bioactmat.2024.08.032.

References

[1] D.L. Coutu, K.D. Kokkaliaris, L. Kunz, T. Schroeder, Three-dimensional map of nonhematopoietic bone and bone-marrow cells and molecules, Nat. Biotechnol. 35 (2017) 1202–1210.
[2] B.O. Zhou, H. Yu, R. Yue, Z. Zhao, J.J. Rios, O. Naveiras, S.J. Morrison, Bone marrow adipocytes promote the regeneration of stem cells and haematopoiesis by secreting SCF, Nat. Cell Biol. 19 (2017) 891–903.
[3] E. Quartin, S. Rosa, S. Gonzalez-Anton, L. Mosteo Lopez, V. Francisco, D. Duarte, C. Lo Celso, R. Pires das Neves, L. Ferreira, Nanoparticle-encapsulated retinoic acid for the modulation of bone marrow hematopoietic stem cell niche, Bioact. Mater. 34 (2024) 311–325.
[4] X. Zhang, D. Cao, L. Xu, Y. Xu, Z. Gao, Y. Pan, M. Jiang, Y. Wei, L. Wang, Y. Liao, Q. Wang, L. Yang, X. Xu, Y. Gao, S. Gao, J. Wang, R. Yue, Harnessing matrix stiffness to engineer a bone marrow niche for hematopoietic stem cell rejuvenation, Cell Stem Cell 30 (2023) 378–395.e8.
[5] O. Naveiras, V. Nardi, P.L. Wenzel, P.V. Hauschka, F. Fahey, G.Q. Daley, Bone-marrow adipocytes as negative regulators of the haematopoietic microenvironment, Nature 460 (2009) 259–263.
[6] A. Krings, S. Rahman, S. Huang, Y. Lu, P.J. Czernik, B. Lecka-Czernik, Bone marrow fat has brown adipose tissue characteristics, which are attenuated with aging and diabetes, Bone 50 (2012) 546–552.
[7] L. Xu, X. Ma, N.K. Verma, D. Wang, O. Gavrilova, R.L. Proia, T. Finkel, E. Mueller, Ablation of PPARγ in subcutaneous fat exacerbates age-associated obesity and metabolic decline, Aging Cell 17 (2018) 1–10.
[8] K. Saeki, M. Nishio, T. Yoneshiro, M. Nakahara, S. Suzuki, K. Saeki, M. Hasegawa, Y. Kawai, H. Akutsu, A. Umezawa, K. Yasuda, K. Tobe, A. Yuo, K. Kubota, M. Saito, Production of functional classical brown adipocytes from human pluripotent stem cells using specific hemopoietin cocktail without gene transfer, Cell Metab. 16 (2012) 394–406.
[9] D. Mattiucci, G. Maurizi, V. Izzi, L. Cenci, M. Ciarlantini, S. Mancini, E. Mensà, R. Pascarella, M. Vivarelli, A. Olivieri, P. Leoni, A. Poloni, Bone marrow adipocytes support hematopoietic stem cell survival, J. Cell. Physiol. 233 (2018) 1500–1511.
[10] Z. Li, J. Hardij, D.P. Bagchi, E.L. Scheller, O.A. MacDougald, Development, regulation, metabolism and function of bone marrow adipose tissues, Bone 110 (2018) 134–140.
[11] J. Tratwal, S. Rojas-Sutterlin, C. Bataclan, S. Blum, O. Naveiras, Bone marrow adiposity and the hematopoietic niche: a historical perspective of reciprocity, heterogeneity, and lineage commitment, Best Pract. Res. Clin. Endocrinol. Metabol. 35 (2021) 101564.
[12] Z. Zhang, Z. Huang, B. Ong, C. Sahu, H. Zeng, H. Bin Ruan, Bone marrow adipose tissue-derived stem cell factor mediates metabolic regulation of hematopoiesis, Haematologica 104 (2019) 1731–1743.
[13] F.J.A. De Paula, C.J. Rosen, Structure and function of bone marrow adipocytes, Compr, Physiol. 8 (2018) 315–349.
[14] F. Louis, Y. Sowa, S. Kitano, M. Matsusaki, High-throughput drug screening models of mature adipose tissues which replicate the physiology of patients' Body Mass Index (BMI), Bioact. Mater. 7 (2022) 227–241.
[15] X. Cahu, J. Calvo, S. Poglio, N. Prade, B. Colsch, M.L. Arcangeli, T. Leblanc, A. Petit, F. Baleydier, A. Baruchel, J. Landman-Parker, C. Junot, J. Larghero, P. Ballerini, E. Delabesse, B. Uzan, F. Pflumio, Bone marrow sites differently imprint dormancy and chemoresistance to T-cell acute lymphoblastic leukemia, Blood Adv 1 (2017) 1760–1772.
[16] A.L. Boyd, J.C. Reid, K.R. Salci, L. Aslostovar, Y.D. Benoit, Z. Shapovalova, M. Nakanishi, D.P. Porras, M. Almakadi, C.J.V. Campbell, M.F. Jackson, C.A. Ross, R. Foley, B. Leber, D.S. Allan, M. Sabloff, A. Xenocostas, T.J. Collins, M. Bhatia, Acute myeloid leukaemia disrupts endogenous myelo-erythropoiesis by compromising the adipocyte bone marrow niche, Nat. Cell Biol. 19 (2017) 1336–1347.
[17] H. Wang, Y. Leng, Y. Gong, Bone marrow fat and hematopoiesis, Front. Endocrinol. 9 (2018) 1–9.
[18] C. Attané, D. Estève, K. Chaoui, J.S. Iacovoni, J. Corre, M. Moutahir, P. Valet, O. Schiltz, N. Reina, C. Muller, Human bone marrow is comprised of adipocytes with specific lipid metabolism, Cell Rep. 30 (2020) 949–958.e6.
[19] J. Zinngrebe, K.-M. Debatin, P. Fischer-Posovszky, Adipocytes in hematopoiesis and acute leukemia: friends, enemies, or innocent bystanders? Leukemia 34 (2020) 2305–2316.
[20] Y. Lee, M. Decker, H. Lee, L. Ding, Extrinsic regulation of hematopoietic stem cells in development, homeostasis and diseases, Wiley Interdiscip. Rev. Dev. Biol. 6 (2017) 1–23.
[21] Z. Huang, H. Bin Ruan, L. Xian, W. Chen, S. Jiang, A. Song, Q. Wang, P. Shi, X. Gu, X. Gao, The stem cell factor/Kit signalling pathway regulates mitochondrial function and energy expenditure, Nat. Commun. 5 (2014) 4282.
[22] K. Dai, Q. Zhang, S. Deng, Y. Yu, F. Zhu, S. Zhang, Y.Z. Pan, D. Long, J. Wang, C. Liu, A BMP-2–triggered in vivo osteo-organoid for cell therapy, Sci. Adv. 9 (2023) 1–16.
[23] K. Dai, W. Zhang, S. Deng, J. Wang, C. Liu, Sulfated polysaccharide regulates the homing of HSPCs in a BMP-2-triggered in vivo osteo-organoid, Adv. Sci. 10 (2023) e2301592.
[24] A. Okuno, H. Tamemoto, K. Tobe, K. Ueki, Y. Mori, K. Iwamoto, K. Umesono, Y. Akanuma, T. Fujiwara, H. Horikoshi, Y. Yazaki, T. Kadowaki, Troglitazone increases the number of small adipocytes without the change of white adipose tissue mass in obese Zucker rats, J. Clin. Invest. 101 (1998) 1354–1361.
[25] D. Ali, L. Chen, J.M. Kowal, M. Okla, M. Manikandan, M. AlShehri, Y. AlMana, R. AlObaidan, N. AlOtaibi, R. Hamam, N.M. Alajez, A. Aldahmash, M. Kassem, M. Alfayez, Resveratrol inhibits adipocyte differentiation and cellular senescence of human bone marrow stromal stem cells, Bone 133 (2020) 115252.
[26] J.H. Choi, A.S. Banks, J.L. Estall, S. Kajimura, P. Boström, D. Laznik, J.L. Ruas, M. J. Chalmers, T.M. Kamenecka, M. Blüher, P.R. Griffin, B.M. Spiegelman, Anti-diabetic drugs inhibit obesity-linked phosphorylation of PPARγ 3 by Cdk5, Nature 466 (2010) 451–456.
[27] O. Wang, L. Han, H. Lin, M. Tian, S. Zhang, B. Duan, S. Chung, C. Zhang, X. Lian, Y. Wang, Y. Lei, Fabricating 3-dimensional human brown adipose microtissues for transplantation studies, Bioact. Mater. 22 (2023) 518–534.
[28] X. Wang, L. Gao, Y. Han, M. Xing, C. Zhao, J. Peng, J. Chang, Silicon-enhanced adipogenesis and angiogenesis for vascularized adipose tissue engineering, Adv. Sci. 5 (2018).
[29] X. Ma, D. Wang, W. Zhao, L. Xu, Deciphering the roles of PPARγ in adipocytes via dynamic change of transcription complex, Front. Endocrinol. 9 (2018) 1–10.
[30] G. Lin, H. Wang, J. Dai, X. Li, M. Guan, S. Gao, Q. Ding, H. Wang, H. Fang, Conjugated linoleic acid prevents age-induced bone loss in mice by regulating both osteoblastogenesis and adipogenesis, Biochem. Biophys. Res. Commun. 490 (2017) 813–820.
[31] S. Rayalam, M.A. Della-Fera, C.A. Baile, Phytochemicals and regulation of the adipocyte life cycle, J. Nutr. Biochem. 19 (2008) 717–726.
[32] T.G. Moreira, L.S. Horta, A.C. Gomes-Santos, R.P. Oliveira, N.M.G.P. Queiroz, D. Mangani, B. Daniel, A.T. Vieira, S. Liu, A.M. Rodrigues, D.A. Gomes, G. Gabriely, E. Ferreira, H.L. Weiner, R.M. Rezende, L. Nagy, A.M.C. Faria, CLA-supplemented diet accelerates experimental colorectal cancer by inducing TGF-β-producing macrophages and T cells, Mucosal Immunol. 12 (2019) 188–199.
[33] C. Wang, Y. Yu, H. Chen, S. Zhang, J. Wang, C. Liu, Construction of cytokine reservoirs based on sulfated chitosan hydrogels for the capturing of VEGF in situ, J. Mater. Chem. B 7 (2019) 1882–1892.
[34] H. Chen, Y. Yu, C. Wang, J. Wang, C. Liu, The regulatory role of sulfated polysaccharides in facilitating rhBMP-2-induced osteogenesis, Biomater. Sci. 7 (2019) 4375–4387.
[35] S. Zhang, J. Chen, Y. Yu, K. Dai, J. Wang, C. Liu, Accelerated bone regenerative efficiency by regulating sequential release of BMP-2 and VEGF and synergism with sulfated chitosan, ACS Biomater. Sci. Eng. 5 (2019) 1944–1955.
[36] S. Kishimoto, S. Nakamura, H. Hattori, S.I. Nakamura, F. Oonuma, Y. Kanatani, Y. Tanaka, Y. Mori, Y. Harada, M. Tagawa, M. Ishihara, Human stem cell factor (SCF) is a heparin-binding cytokine, J. Biochem. 145 (2009) 275–278.
[37] K.J. Suchacki, A.A.S. Tavares, D. Mattiucci, E.L. Scheller, G. Papanastasiou, C. Gray, M.C. Sinton, L.E. Ramage, W.A. McDougald, A. Lovdel, R.J. Sulston, B. J. Thomas, B.M. Nicholson, A.J. Drake, C.J. Alcaide-Corral, D. Said, A. Poloni, S. Cinti, G.J. Macpherson, M.R. Dweck, J.P.M. Andrews, M.C. Williams, R. J. Wallace, E.J.R. van Beek, O.A. MacDougald, N.M. Morton, R.H. Stimson, W. P. Cawthorn, Bone marrow adipose tissue is a unique adipose subtype with distinct roles in glucose homeostasis, Nat. Commun. 11 (2020).
[38] B.B. Brandão, S. Madsen, A. Rabiee, M. Oliverio, G.P. Ruiz, D.L. Ferrucci, J. L. Branquinho, D. Razolli, S. Pinto, T.S. Nielsen, W.T. Festuccia, A.S. Martins, B. A. Guerra, T.L. Knittel, D. Søgaard, S. Larsen, J.W. Helge, J. Brandauer, L. A. Velloso, B. Emanuelli, J.W. Kornfeld, C.R. Kahn, S.G. Vienberg, J.R. Zierath, J. T. Treebak, M.A. Mori, Dynamic changes in DICER levels in adipose tissue control metabolic adaptations to exercise, Proc. Natl. Acad. Sci. U.S.A. 117 (2020) 23932–23941.
[39] B.A. Shook, R.R. Wasko, O. Mano, M. Rutenberg-Schoenberg, M.C. Rudolph, B. Zirak, G.C. Rivera-Gonzalez, F. López-Giráldez, S. Zarini, A. Rezza, D.A. Clark, M. Rendl, M.D. Rosenblum, M.B. Gerstein, V. Horsley, Dermal adipocyte lipolysis and myofibroblast conversion are required for efficient skin repair, Cell Stem Cell 26 (2020) 880–895.e6.
[40] D. Kong, L. Peng, M. Bosch-Fortea, A. Chrysanthou, C.V.J.M. Alexis, C. Matellan, A. Zarbakhsh, G. Mastroianni, A. del Rio Hernandez, J.E. Gautrot, Impact of the multiscale viscoelasticity of quasi-2D self-assembled protein networks on stem cell expansion at liquid interfaces, Biomaterials 284 (2022) 121494.
[41] D. Indana, P. Agarwal, N. Bhutani, O. Chaudhuri, Viscoelasticity and adhesion signaling in biomaterials control human pluripotent stem cell morphogenesis in 3D culture, Adv. Mater. 33 (2021) 1–16.
[42] T. Bai, J. Li, A. Sinclair, S. Imren, F. Merriam, F. Sun, M.B. O'Kelly, C. Nourigat, P. Jain, J.J. Delrow, R.S. Basom, H.C. Hung, P. Zhang, B. Li, S. Heimfeld, S. Jiang, C. Delaney, Expansion of primitive human hematopoietic stem cells by culture in a zwitterionic hydrogel, Nat. Med. 25 (2019) 1566–1575.

[43] A.C. Wilkinson, R. Ishida, H. Nakauchi, S. Yamazaki, Long-term ex vivo expansion of mouse hematopoietic stem cells, Nat. Protoc. 15 (2020) 628–648.
[44] N. Huebsch, P.R. Arany, A.S. Mao, D. Shvartsman, O.A. Ali, S.A. Bencherif, J. Rivera-Feliciano, D.J. Mooney, Harnessing traction-mediated manipulation of the cell/matrix interface to control stem-cell fate, Nat. Mater. 9 (2010) 518–526.
[45] M. Nii, J.H. Lai, M. Keeney, L.H. Han, A. Behn, G. Imanbayev, F. Yang, The effects of interactive mechanical and biochemical niche signaling on osteogenic differentiation of adipose-derived stem cells using combinatorial hydrogels, Acta Biomater. 9 (2013) 5475–5483.
[46] R. Yue, B.O. Zhou, I.S. Shimada, Z. Zhao, S.J. Morrison, Leptin receptor promotes adipogenesis and reduces osteogenesis by regulating mesenchymal stromal cells in adult bone marrow, Cell Stem Cell 18 (2016) 782–796.
[47] E.L. Scheller, C.R. Doucette, B.S. Learman, W.P. Cawthorn, S. Khandaker, B. Schell, B. Wu, S.Y. Ding, M.A. Bredella, P.K. Fazeli, B. Khoury, K.J. Jepsen, P.F. Pilch, A. Klibanski, C.J. Rosen, O.A. MacDougald, Region-specific variation in the properties of skeletal adipocytes reveals regulated and constitutive marrow adipose tissues, Nat. Commun. 6 (2015) 1–13.
[48] Q. Zhang, Y. Liu, J. Li, J. Wang, C. Liu, Recapitulation of growth factor-enriched microenvironment via BMP receptor activating hydrogel, Bioact. Mater. 20 (2023) 638–650.
[49] B. Guo, X. Huang, M.R. Lee, S.A. Lee, H.E. Broxmeyer, Antagonism of PPAR-γ 3 signaling expands human hematopoietic stem and progenitor cells by enhancing glycolysis, Nat. Med. 24 (2018) 360–367.
[50] Y. Kfoury, D.T. Scadden, Mesenchymal cell contributions to the stem cell niche, Cell Stem Cell 16 (2015) 239–253.
[51] P.E. Bourgine, T. Klein, A.M. Paczulla, T. Shimizu, L. Kunz, K.D. Kokkaliaris, D. L. Coutu, C. Lengerke, R. Skoda, T. Schroeder, I. Martin, In vitro biomimetic engineering of a human hematopoietic niche with functional properties, Proc. Natl. Acad. Sci. U.S.A. 115 (2018) E5688–E5695.
[52] B.R. Chitteti, Y.H. Cheng, B. Poteat, S. Rodriguez-Rodriguez, W.S. Goebel, N. Carlesso, M.A. Kacena, E.F. Srour, Impact of interactions of cellular components of the bone marrow microenvironment on hematopoietic stem and progenitor cell function, Blood 115 (2010) 3239–3248.
[53] A. Shaaban, L. Gaur, J.A. Thomson, D. Rajesh, FGF-2 supplementation enhances hematopoietic differentiation of rhesus ESC's, Blood 108 (2006) 1667, 1667.
[54] L.D. Thompson, M.W. Pantoliano, B.A. Springer, Energetic characterization of the basic fibroblast growth factor-heparin interaction: identification of the heparin binding domain, Biochemistry 33 (1994) 3831–3840.
[55] P. Lee, C.D. Werner, E. Kebebew, F.S. Celi, Functional thermogenic beige adipogenesis is inducible in human neck fat, Int. J. Obes. 38 (2014) 170–176.
[56] H.-P. Gerber, A.K. Malik, G.P. Solar, D. Sherman, X.H. Liang, G. Meng, K. Hong, J. C. Marsters, N. Ferrara, VEGF regulates haematopoietic stem cell survival by an internal autocrine loop mechanism, Nature 417 (2002) 954–958.
[57] A. Sebollela, T.C. Cagliari, G.S.C.S. Limaverde, A. Chapeaurouge, M.H.F. Sorgine, T. Coelho-Sampaio, C.H.I. Ramos, S.T. Ferreira, Heparin-binding sites in granulocyte-macrophage colony-stimulating factor, J. Biol. Chem. 280 (2005) 31949–31956.
[58] C.L. Li, G.R. Johnson, Stimulation of multipotential, erythroid and other murine haematopoietic progenitor cells by adherent cell lines in the absence of detectable multi-CSF (IL-3), Nature 316 (1985) 633–636.
[59] D. Merrick, A. Sakers, Z. Irgebay, C. Okada, C. Calvert, M.P. Morley, I. Percec, P. Seale, Identification of a mesenchymal progenitor cell hierarchy in adipose tissue, Science 80 (2019) 364.
[60] K. Dai, T. Shen, Y. Yu, S. Deng, L. Mao, J. Wang, Biomaterials Generation of rhBMP-2-induced juvenile ossicles in aged mice, Biomaterials 258 (2020) 120284.
[61] M.C.R. Cunha, F. da S. Lima, M.A.R. Vinolo, A. Hastreiter, R. Curi, P. Borelli, R. A. Fock, Protein malnutrition induces bone marrow mesenchymal stem cells commitment to adipogenic differentiation leading to hematopoietic failure, PLoS One 8 (2013) 1–12.
[62] B.O. Zhou, R. Yue, M.M. Murphy, J.G. Peyer, S.J. Morrison, Leptin-receptor-expressing mesenchymal stromal cells represent the main source of bone formed by adult bone marrow, Cell Stem Cell 15 (2014) 154–168.
[63] A. Franz, W. Wood, P. Martin, Fat body cells are motile and actively migrate to wounds to drive repair and prevent infection, Dev. Cell 44 (2018) 460–470.e3.
[64] M. Shao, C. Hepler, Q. Zhang, B. Shan, L. Vishvanath, G.H. Henry, S. Zhao, Y.A. An, Y. Wu, D.W. Strand, R.K. Gupta, Pathologic HIF1α signaling drives adipose progenitor dysfunction in obesity, Cell Stem Cell (2021) 1–17.
[65] B. Ortiz, L. Wassef, E. Shabrova, L. Cordeddu, S. Banni, L. Quadro, Hepatic retinol secretion and storage are altered by dietary CLA: common and distinct actions of CLA c9,t11 and t10,c12 isomers, J. Lipid Res. 50 (2009) 2278–2289.
[66] Y. Fan, Y. Fang, L. Ma, H. Jiang, Investigation of micellization and vesiculation of conjugated linoleic acid by means of self-assembling and self-crosslinking, J. Surfactants Deterg. 18 (2015) 179–188.
[67] X. Zhang, Y. Liu, S. Zhang, T. Shen, J. Wang, C. Liu, Potentiation effect on accelerating diabetic wound healing using 2- N ,6- O -sulfated chitosan-doped PLGA scaffold, RSC Adv. 8 (2018) 19085–19097.
[68] C. McGown, A. Birerdinc, Z.M. Younossi, Adipose tissue as an endocrine organ, Clin. Liver Dis. 18 (2014) 41–58.
[69] B. Liu, P. Lv, X. Zhang, C. Xia, X. Liu, J. Liu, J. Xue, Q. He, S. Qin, Zn-Fe primary battery-enabled controlled hydrogen release in stomach for improving insulin resistance in obesity-associated type 2 diabetes, Bioact. Mater. 33 (2024) 242–250.
[70] L. Priscilla, C. Yoo, S. Jang, S. Park, G. Lim, T. Kim, D.Y. Lee, Immunotherapy targeting the obese white adipose tissue microenvironment: focus on non-communicable diseases, Bioact. Mater. 35 (2024) 461–476.
[71] L. Zhong, L. Yao, R. Tower, Y. Wei, Z. Miao, J. Park, R. Shrestha, L. Wang, W. Yu, N. Holdreith, Y. Zhang, W. Tong, Y. Gong, F. Long, J. Ahn, P. Seale, K. Susztak, M. Li, C. Chen, L. Qin, Single cell transcriptomics identifies a unique adipose lineage cell population that regulates bone marrow environment, eLife. 9 (2020) e54695.
[72] B. Dai, X. Li, J. Xu, Y. Zhu, L. Huang, W. Tong, H. Yao, D.H. Chow, L. Qin, Synergistic effects of magnesium ions and simvastatin on attenuation of high-fat diet-induced bone loss, Bioact. Mater. 6 (2021) 2511–2522.
[73] H. Wang, M. Willershäuser, A. Karlas, D. Gorpas, J. Reber, V. Ntziachristos, S. Maurer, T. Fromme, Y. Li, M. Klingenspor, A dual Ucp1 reporter mouse model for imaging and quantitation of brown and brite fat recruitment, Mol. Metabol. 20 (2019) 14–27.
[74] C. Sugiura, G. Zheng, L. Liu, K. Sayama, Catechins and caffeine promote lipid metabolism and heat production through the transformation of differentiated 3T3-L1 adipocytes from white to beige adipocytes, J. Food Sci. 85 (2020) 192–200.
[75] P. Xi, J. Xue, Z. Wu, H. Wang, J. Han, H. Liang, D. Tian, Liver kinase B1 induces browning phenotype in 3 T3-L1 adipocytes, Gene 682 (2019) 33–41.
[76] K. Dai, S. Deng, Y. Yu, F. Zhu, J. Wang, C. Liu, Construction of developmentally inspired periosteum-like tissue for bone regeneration, Bone Res. 10 (2022) 1.
[77] S. Deng, F. Zhu, K. Dai, J. Wang, C. Liu, Harvest of functional mesenchymal stem cells derived from in vivo osteo-organoids, Biomater. Transl. 4 (2023) 270–279.